

Enhanced biological carbon consumption in a high CO₂ ocean

U. Riebesell¹, K. G. Schulz¹, R. G. J. Bellerby^{2,3}, M. Botros¹, P. Fritsche¹, M. Meyerhöfer¹, C. Neill², G. Nondal^{2,3}, A. Oschlies¹, J. Wohlers¹ & E. Zöllner¹

The oceans have absorbed nearly half of the fossil-fuel carbon dioxide (CO₂) emitted into the atmosphere since pre-industrial times¹, causing a measurable reduction in seawater pH and carbonate saturation². If CO₂ emissions continue to rise at current rates, upper-ocean pH will decrease to levels lower than have existed for tens of millions of years and, critically, at a rate of change 100 times greater than at any time over this period³. Recent studies have shown effects of ocean acidification on a variety of marine life forms, in particular calcifying organisms^{4–6}. Consequences at the community to ecosystem level, in contrast, are largely unknown. Here we show that dissolved inorganic carbon consumption of a natural plankton community maintained in mesocosm enclosures at initial CO₂ partial pressures of 350, 700 and 1,050 μatm increases with rising CO₂. The community consumed up to 39% more dissolved inorganic carbon at increased CO₂ partial pressures compared to present levels, whereas nutrient uptake remained the same. The stoichiometry of carbon to nitrogen drawdown increased from 6.0 at low CO₂ to 8.0 at high CO₂, thus exceeding the Redfield carbon:nitrogen ratio of 6.6 in today's ocean⁷. This

by about a factor of two relative to the present value (380 μatm), and could increase by a factor of three by the middle of the next century¹⁰. This will cause seawater pH to further drop by 0.3 and 0.6 pH units, respectively, in addition to the 0.12 pH-unit decrease that has occurred since pre-industrial times³. Changes in seawater chemistry of this magnitude are expected to have adverse effects, not only on individual species but also at the community and ecosystem level¹¹.

To investigate the effect of rising CO₂ on a natural plankton community, we conducted a mesocosm CO₂ perturbation study in the Raune Fjord in southern Norway. Nine enclosures, each containing 27 m³ of ambient water, were aerated with CO₂-enriched air to achieve concentrations of 350 μatm (1 × CO₂), 700 μatm (2 × CO₂) and 1,050 μatm (3 × CO₂). After nutrient addition, the development and decline of a plankton bloom was monitored over 24 days.

A rapid decline in CO₂ partial pressures (*p*_{CO₂}) owing to photosynthetic carbon fixation led to a minimum *p*_{CO₂} at day 12, at which point nitrate concentrations were close to exhaustion (Fig. 1). The greater drop in *p*_{CO₂} at increased CO₂ levels was caused by the lower buffer capacity of sea water under these conditions. No difference

View metadata, citation and similar papers at core.ac.uk

brought to you by  CORE

provided by OceanRep

is applicable to the natural environment, the observed responses have implications for a variety of marine biological and biogeochemical processes, and underscore the importance of biologically driven feedbacks in the ocean to global change.

Throughout Earth's history, the ocean has had a crucial role in modulating atmospheric carbon dioxide through a variety of physical, chemical and biological processes. The same processes are involved in the ocean's response to anthropogenic perturbations of the global carbon cycle. A key process responsible for about three-quarters of the surface to deep-ocean gradient in dissolved inorganic carbon (DIC) is the biological carbon pump⁸. This transports carbon bound by photosynthesis from the sunlit surface layer to the deep ocean. Integrated over the global ocean, the biotically driven surface to deep-ocean DIC gradient of ~220 μmol kg⁻¹ (ref. 9) amounts to ~2,500 petagrams of carbon (Pg C) (1 Pg = 10¹⁵ g), that is, 3.5 times the atmospheric carbon pool. Small changes in this pool, for example, caused by biological responses to ocean change, would have a strong effect on atmospheric CO₂.

At present, one of the most far-reaching global perturbations of the marine environment is caused by the massive invasion of fossil fuel CO₂ into the ocean, making it the second largest sink for anthropogenic carbon dioxide after the atmosphere itself. CO₂ entering the ocean alters the seawater carbonate equilibrium, decreasing pH and shifting dissolved inorganic carbon away from carbonate (CO₃²⁻) towards more bicarbonate (HCO₃⁻) and CO₂. For a 'business-as-usual' emission scenario in the year 2100 (IS92a), the CO₂ concentration will rise

Phytoplankton biomass, depicted by chlorophyll *a* concentrations (Fig. 1b), peaked on day 10. This corresponded to the maximum in particulate organic carbon (Methods, Supplementary Fig. 2) and coincided with phosphate exhaustion. The phytoplankton bloom was initially dominated by diatoms, which reached a maximum 1–2 days before the peak of the bloom owing to silicate limitation on day 9 (Fig. 2). This was followed by a dominance of the prymnesiophytes, primarily the coccolithophore *Emiliania huxleyi*, which had maximum cell abundances of (3.5–6.2) × 10⁶ cells l⁻¹ on days 10–11. Whereas diatoms and prymnesiophytes accounted for 85–90% of phytoplankton biomass during the bloom, prasinophytes, dinoflagellates and cyanobacteria dominated after the decline of the bloom. Neither phytoplankton composition nor succession differed significantly between CO₂ treatments.

A distinct CO₂ treatment effect is evident for cumulative DIC drawdown owing to production of organic matter (ΔDIC_{org}, Fig. 3a), averaging 79, 100 and 110 μmol kg⁻¹ at the peak of the bloom (day 12) in water at 1 × CO₂, 2 × CO₂ and 3 × CO₂ concentration, respectively. Thus, for the same uptake of inorganic nutrients, net community carbon consumption under increased CO₂ exceeded present rates by 27% (2 × CO₂) and 39% (3 × CO₂). Continuous oxygen measurements in mesocosms 2 (3 × CO₂), 5 (2 × CO₂) and 8 (1 × CO₂), which revealed up to 20 μmol kg⁻¹ higher O₂ concentrations at increased CO₂ (data not shown), indicate enhanced net photosynthesis to be the source of the observed CO₂ effect. Possible causes for this include increased photosynthetic

¹Leibniz Institute of Marine Sciences, IFM-GEOMAR, 24105 Kiel, Germany. ²Bjerknes Centre for Climate Research, ³Geophysical Institute, University of Bergen, Allégaten 70, 5007 Bergen, Norway.

carbon fixation owing to lower energetic cost of carbon acquisition, reduced photorespiration owing to a higher $\text{CO}_2:\text{O}_2$ ratio, and decreased organic matter degradation, for example, owing to changes in food quality.

Whereas the cumulative carbon to nitrate (C:N) drawdown remained slightly below the Redfield C:N ratio of 6.6 under $1 \times \text{CO}_2$ (Fig. 3c), this ratio increased to 7.1 and 8.0 under $2 \times \text{CO}_2$ and $3 \times \text{CO}_2$, respectively. The ratio of particulate organic carbon to particulate organic nitrogen (POC/PON) accumulating in the surface layer, in contrast, closely adhered to the Redfield C:N ratio independent of CO_2 treatment (see Methods, Supplementary Fig. 2). Deviation of DIC/NO_3^- drawdown from POC/PON build-up, previously reported from both mesocosm and field studies^{12,13}, was attributed to dissolved organic carbon (DOC) release¹⁴. DOC concentrations also increased during bloom development in our study, but surface-layer DOC accumulations of $\sim 25 \mu\text{mol kg}^{-1}$ remained well below levels expected from the difference between DIC drawdown and POC build-up (see below). A possible fate of DOC is indicated by a fourfold increase in the concentration of transparent exopolymer particles (TEP), which are known to originate from dissolved precursors and to accelerate particle aggregation and sinking¹⁵.

The loss of organic carbon from the upper mixed layer (UML) through sinking is given by the difference between DIC drawdown and build-up of POC and DOC, $\Delta C_{\text{loss}} = \Delta \text{DIC}_{\text{org}} - (\Delta C_{\text{POC}} + \Delta C_{\text{DOC}})$. Between 15% and 30% of organically fixed carbon was lost from the UML daily, with consistently higher loss rates at increased CO_2 (Fig. 3b). The 12-day cumulative carbon loss at $3 \times \text{CO}_2$ exceeded that under $1 \times \text{CO}_2$ by about $30 \mu\text{mol kg}^{-1}$, which closely resembles the difference in net inorganic carbon drawdown between

the lowest and highest CO_2 treatment. Enhanced particle sinking at increased CO_2 may explain why POC and TEP concentrations did not show a significant difference between treatments. In fact, positive correlations between TEP production and CO_2 concentration were observed in natural plankton assemblages dominated by diatoms and cyanobacteria¹⁶ and in batch culture incubations with *E. huxleyi*¹⁷.

The extent to which the observed CO_2 sensitivity in phytoplankton carbon consumption and stoichiometry in carbon-to-nutrient drawdown can be extrapolated to other marine ecosystems remains to be seen. In accordance with our results, enhanced carbon fixation of up to 15% in response to three-times increased CO_2 was observed during incubations of natural phytoplankton assemblages from the nutrient-poor central Atlantic¹⁸. Higher carbon-to-nitrate drawdown at increased CO_2 concentrations also occurred in a previous mesocosm CO_2 perturbation experiment during a bloom of *E. huxleyi*¹⁹. The concordant results indicate the existence of a widespread mechanism under high CO_2 conditions. The phytoplankton groups dominating in the mesocosm studies—diatoms and coccolithophores—are also the main primary producers in high productivity areas and are the principal drivers of biologically induced carbon export to the deep sea.

Apart from seawater acidification, the ocean in a high CO_2 world will experience other changes, including higher surface temperatures, enhanced stratification and decreased mixed-layer depths. Although the direct effect of rising temperatures on net community carbon-to-nutrient ratios is unclear, at the organism level most experimental

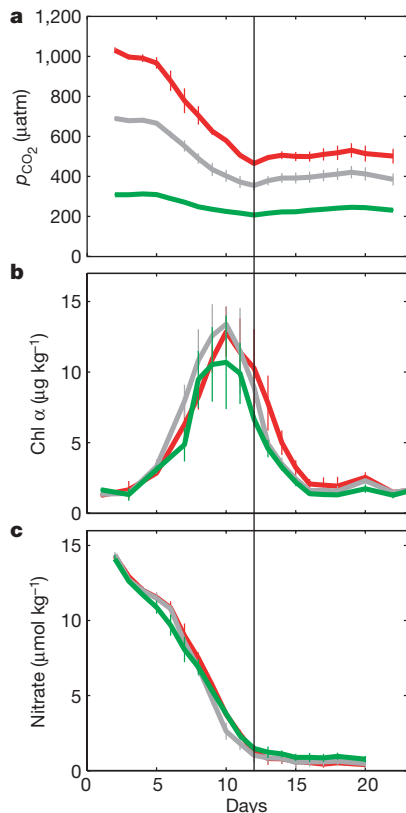


Figure 1 | Growth conditions in experimental mesocosms. **a**, CO_2 partial pressures (p_{CO_2}); **b**, chlorophyll *a* concentrations (Chl *a*); and **c**, nitrate concentrations in the upper 5.5 m mixed layer (UML) during the experiment. Values are means of triplicate CO_2 treatments with initial p_{CO_2} of 350 μatm (green), 700 μatm (grey) and 1,050 μatm (red). Error bars denote ± 1 standard deviation. The vertical line indicates time of deep water injection into UML owing to vertical mixing (day 12).

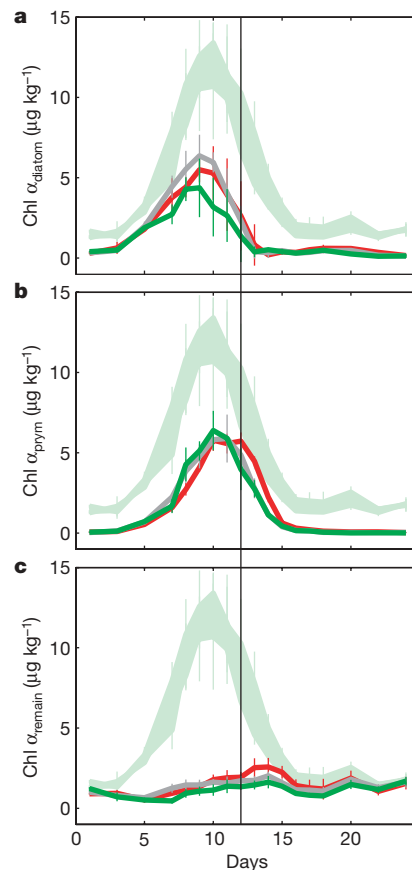


Figure 2 | Development of dominant phytoplankton groups. Chlorophyll *a* equivalents in the UML of: **a**, diatoms (Chl a_{diatom}); **b**, prymnesiophytes (Chl a_{pym}), predominantly the coccolithophore *E. huxleyi*; and **c**, remaining chlorophyll *a* (Chl a_{remain}), primarily containing prasinophytes, dinoflagellates and cyanobacteria. Group-specific chlorophyll *a* equivalents were derived from high-performance liquid chromatography pigment analysis using CHEMTAX algorithms (for details see Methods). The light-green curve represents the range of total chlorophyll *a* as depicted in Fig. 1b. Colour code is as in Fig. 1. The vertical line indicates time of deep water injection into UML owing to vertical mixing (day 12). Error bars denote ± 1 standard deviation.

studies indicate an increase in the C:N ratio with increasing temperature²⁰. Decreased mixed-layer depth tends to increase phytoplankton carbon-to-nutrient ratios²¹, which would augment the direct CO₂ effect on C:N:P stoichiometry observed in this study. Increased stratification, in contrast, would decrease the supply of nutrients to the surface layer, reducing overall primary and export production. Thus, concurrent with a decrease in the strength of the biological pump caused by a lower nutrient supply, the pump's efficiency is likely to increase at increased CO₂.

Shifting of the C:N:P stoichiometry of marine primary production has long been recognized as one of the most powerful mechanisms determining ocean-atmosphere carbon partitioning²². Carbon relative to nitrogen drawdown in excess of the Redfield C:N ratio, often referred to as carbon over-consumption²³, is reported for various oceanographic regimes^{12,13,23,24}, but was generally considered to be a transient phenomenon. Whether this also applies to the observed CO₂ sensitivity of plankton carbon consumption and to what extent the mechanism(s) underlying this trend are applicable to other diatom- and coccolithophore-dominated new production systems is presently unknown. Assuming the observed response can be extrapolated to new production systems in the ocean, we calculate an excess CO₂ sequestration potential by the biological carbon pump of 116 Pg C until 2100 (for details see Methods). The efficiency of this negative feedback mechanism develops only gradually with rising

CO₂, reaching its maximum strength long after atmospheric CO₂ has transgressed to levels tolerable with regard to climate change and ocean acidification.

Aside from its effect on oceanic carbon sequestration, a more efficient biological carbon pump would lead to an expansion of deep ocean oxygen minimum zones with possible consequences for marine biogeochemical cycling. Increasing C:N ratios would also lower the nutritional value of primary-produced organic matter, which may affect the efficiency of bacterial degradation and zooplankton reproduction²⁵, thus having further implications for marine ecosystem dynamics. Changing carbon-to-nutrient ratios in oceanic primary and export production may thereby act as a forceful driver for ecosystem processes and biogeochemical cycles in the future ocean.

METHODS SUMMARY

The study was conducted between 15 May and 9 June 2005 at the Espesgrend Marine Biological Station (at Raunefjorden, 60.3° N, 5.2° E) of the University of Bergen, Norway. Nine polyethylene mesocosm enclosures (~27 m³, 9.5 m water depth) were moored to a raft, and filled with unfiltered, nutrient-poor, post-bloom fjord water pumped from 13.5 m depth adjacent to the raft. The enclosures were covered by gas-tight tents made of ethylene tetrafluoroethylene foil, which allowed for 95% light transmission of the complete spectrum of sunlight.

The carbonate system in the mesocosms was manipulated by CO₂ aeration to obtain triplicates of three concentrations, 350 μatm (1 × CO₂), 700 μatm (2 × CO₂) and 1,050 μatm (3 × CO₂) (for details see ref. 19). CO₂ aeration of the water column was ended after 3 days, when target CO₂ levels were reached. Continuous flushing of the tents with air adjusted at target CO₂ concentrations ensured that starting values were maintained in the overlying air throughout the experiment.

The water column was stratified by addition and subsequent mixing of 800 litres of freshwater into the upper 5.5 m of the mesocosms, resulting in a salinity (S) gradient of 1.5 p.s.u. between the surface mixed layer (S = 30.6 p.s.u.) and the underlying water column. Continuous mixing of this upper layer by peristaltic pumps (flow rate 450 l h⁻¹) maintained a homogenous distribution of dissolved compounds. To promote the development of a phytoplankton bloom, nitrate and phosphate were added to yield initial concentrations of 14 μmol l⁻¹ NO₃⁻ and 0.7 μmol l⁻¹ PO₄³⁻. Owing to left-over silicate in post-bloom waters, the experiment started at a Si(OH)₄ concentration of 3.2 μmol l⁻¹. After nutrient addition, the development and decline of a phytoplankton bloom was closely monitored over a 24-day period (for details on sampling and measurements see Methods).

Full Methods and any associated references are available in the online version of the paper at www.nature.com/nature.

Received 16 June; accepted 17 September 2007.

Published online 11 November 2007.

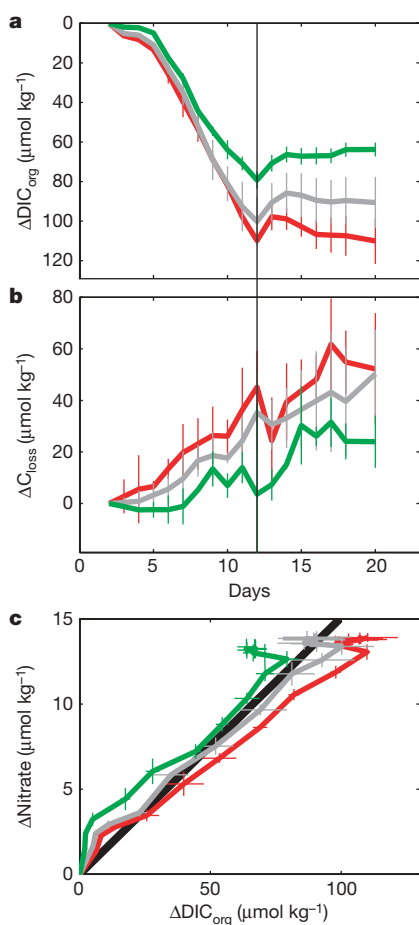


Figure 3 | CO₂ sensitivity of carbon consumption and carbon loss. **a**, Drawdown of dissolved inorganic carbon owing to organic matter production ($\Delta\text{DIC}_{\text{org}}$) in the upper 5.5 m mixed layer (UML) with time. **b**, Loss of organically bound carbon ($\Delta\text{C}_{\text{loss}}$) from the UML with time. The vertical line in **a** and **b** indicates time of deep water injection into UML owing to vertical mixing (day 12). **c**, $\Delta\text{DIC}_{\text{org}}$ versus nitrate drawdown in the UML. The black line represents Redfield C:N ratio of 6.6. Values are means of triplicate CO₂ treatments. Error bars denote ± 1 standard deviation; colour code is as in Fig. 1.

1. Sabine, C. L. *et al.* The oceanic sink for anthropogenic CO₂. *Science* **305**, 367–371 (2004).
2. Feely, R. A. *et al.* Impact of anthropogenic CO₂ on the CaCO₃ system in the oceans. *Science* **305**, 362–366 (2004).
3. Caldeira, K. & Wickett, M. E. Anthropogenic carbon and ocean pH. *Nature* **425**, 365 (2003).
4. Langdon, C. *et al.* Effect of elevated CO₂ on the community metabolism of an experimental coral reef. *Glob. Biogeochem. Cycles* **17**, 1011 (2003).
5. Gattuso, J.-P., Frankignoulle, M., Bourge, I., Romaine, S. & Buddemeier, R. W. Effect of calcium carbonate saturation of seawater on coral calcification. *Glob. Planet. Change* **18**, 37–46 (1998).
6. Riebesell, U. & Zondervan, I. Rost, B. Tortell, P. D., Zeebe, R. E. & Morel, F. M. M. Reduced calcification in marine plankton in response to increased atmospheric CO₂. *Nature* **407**, 634–637 (2000).
7. Redfield, A. C., Ketchum, B. H. & Richards, F. A. in *The Sea* 2nd edn (ed. Hill, M. N.) 26–77 (Wiley, New York, 1963).
8. Volk, T. & Hoffert, M. I. in *The Carbon Cycle and Atmospheric CO₂: Natural Variations Archean to Present* (eds Sunquist, E. T. & Broecker, W. S.) Monograph Vol. 32 99–110 (Am. Geophys. Union, Washington DC, 1985).
9. Gruber, N. & Sarmiento, J. L. in *The Sea: Biological-Physical Interactions in the Oceans* Vol. 12 (eds Robinson, A. R., McCarthy, J. J. & Rothschild, B. J.) 337–399 (Wiley, New York, 2002).
10. Houghton, J. T., *et al.* *Climate Change 2001: The Scientific Basis* (Cambridge Univ. Press, Cambridge, UK, 2001).
11. Raven, J. *et al.* Ocean acidification due to increasing atmospheric carbon dioxide. Policy Document 12/05. *Roy. Soc. Rep.* **12** (2005).
12. Antia, N. J., McAllister, C. D., Parsons, T. R., Stephens, K. & Strickland, J. D. H. Further measurements of primary production using a large-volume plastic sphere. *Limnol. Oceanogr.* **8**, 166–183 (1963).

13. Sambrotto, R. N. *et al.* Elevated consumption of carbon relative to nitrogen in the surface ocean. *Nature* **363**, 248–250 (1993).
14. Banse, K. Uptake of inorganic carbon and nitrate by marine plankton and the Redfield ratio. *Glob. Biogeochem. Cycles* **8**, 81–84 (1994).
15. Engel, A., Thoms, S., Riebesell, U., Rochelle-Newall, E. & Zondervan, I. Polysaccharide aggregation as a potential sink of marine dissolved organic carbon. *Nature* **428**, 929–932 (2004).
16. Engel, A. Direct relationship between CO₂ uptake and transparent exopolymer particles production in natural phytoplankton. *J. Plankton Res.* **24**, 49–53 (2002).
17. Heemann, C. *Phytoplanktonexsudation in Abhängigkeit von der Meerwasserkarbonatchemie*. Thesis, Univ. Bremen (2002).
18. Hein, M. & Sand-Jensen, K. CO₂ increases oceanic primary production. *Nature* **388**, 526–527 (1997).
19. Engel, A. *et al.* Testing the direct effect of CO₂ concentration on a bloom of the coccolithophorid *Emiliania huxleyi* in mesocosm experiments. *Limnol. Oceanogr.* **50**, 493–504 (2005).
20. Woods, H. A. *et al.* Temperature and the chemical composition of poikilothermic organisms. *Funct. Ecol.* **17**, 237–245 (2003).
21. Diehl, S., Berger, S. & Wörhl, R. Flexible algal nutrient stoichiometry mediates environmental influences on phytoplankton and its abiotic resources. *Ecology* **6**, 2931–2945 (2005).
22. Broecker, W. S. Ocean geochemistry during glacial time. *Geochim. Cosmochim. Acta* **46**, 1689–1705 (1982).
23. Toggweiler, J. R. Carbon overconsumption. *Nature* **363**, 210–211 (1993).
24. Körtzinger, A., Koeve, W., Kähler, P. & Mintrop, L. C:N ratios in the mixed layer during the productive season in the Northeast Atlantic Ocean. *Deep-sea Res.* **1** **48**, 661–688 (2001).
25. Sterner, R. W. & Elser, J. J. (eds) *Ecological Stoichiometry* (Princeton Univ. Press, Princeton, 2002).

Supplementary Information is linked to the online version of the paper at www.nature.com/nature.

Acknowledgements We thank the participants of the Pelagic Ecosystem CO₂ Enrichment study (PeECE III, <http://peece.ifm-geomar.de>). We acknowledge J. Egge, J. Nejtgaard and the staff of the Espeyrend Marine Biological Station for helping to organize and set up the mesocosms. This work was supported by the EU projects CARBOOCEAN 'Marine carbon sources and sinks assessment' (GOCE), CABANERA and University of Bergen (LOCUS) funding.

Author Information Reprints and permissions information is available at www.nature.com/reprints. Correspondence and requests for materials should be addressed to U.R. (uribesell@ifm-geomar.de).

METHODS

Sampling. Depth-integrated water samples were taken daily at 10:00 by means of a 5-m long, 6-cm diameter tube that was lowered into the mesocosms, closed at the top, pulled up onto the raft and emptied into sampling bottles. Vertical profiles of temperature and salinity inside the mesocosms were obtained using a hand-operated CTD (SAIV A/S, model SD204).

Measurements. CO₂ partial pressure in seawater and the overlying air was measured using an infrared gas analyser (Li-Cor 6262) coupled to an equilibrator²⁶. The pCO₂ system was mounted on a cart that was moved between the mesocosms. Water was pumped from the mesocosm at 2 litre min⁻¹ and returned to the mesocosm after passing through the equilibrator. Temperature at the inlet of the pump and in the equilibrator was measured simultaneously using platinum RTD digital thermometers. The system was calibrated before and after water analyses with air standards with nominal mixing ratios of 345, 415 and 1,100 p.p.m. Immediately after each measurement of pCO₂, samples for total alkalinity and DIC were taken using the same water pump to fill bottles with ground glass stoppers. Total alkalinity and DIC samples were poisoned with HgCl₂ on collection and were filtered through glass fibre (GF/F) filters before analysis. Total alkalinity was measured using the classical Gran electrotitration method²⁷. The reproducibility of measurements was usually within 4 μmol kg⁻¹. DIC was measured by colometric titration²⁸ with a precision of 2 μmol kg⁻¹.

For the analysis of phytoplankton pigments, 250–500 ml of the water samples were filtered through 25 mm Whatman GF/F filters. Filters were frozen at -20 °C until analysis. For pigment extraction, filters were homogenized in plastic vials (11 ml) together with 1 ml acetone (100%) and a mixture of glass beads (2 and 4 mm) by shaking (5 min) in a cooled Vibrogen cell mill. The extracts were centrifuged (~850 g/5,000 r.p.m. for 10 min, cooled at -10 °C). The extraction process was performed under dimmed light to prevent photo-oxidation of the pigments. Concentrations of pigments (chlorophyll and carotenoids) were determined by reverse-phase high-performance liquid chromatography²⁹. Identification of pigments was carried out by comparing their retention times and absorption spectra obtained with a diode array spectrophotometer (WATERS) with those of pigment standards. Calibration was carried out with commercially available standards. Calculation of the composition of the phytoplankton communities was executed using the CHEMTAX program³⁰, converting the concentrations of marker pigments to equivalents of chlorophyll *a* with suitable pigment-to-chlorophyll *a* ratios.

Nitrate, nitrite, phosphate and silicate were determined from GF/F-filtered samples with an autoanalyser (AA II)³¹. Ammonium was measured according to ref. 32. POC and PON were measured on 0.25 litre or 0.5 litre samples filtered gently (200 mbar) through precombusted (450 °C, 5 h) glass fibre filters (GF/F, Whatman). Filters were fumed overnight with saturated HCl to remove all particulate inorganic carbon, dried for 6 h at 60 °C and measured on an elemental analyser (EuroEA 3000, EuroVector). DOC was measured using the high-temperature catalytic oxidation method³³.

Calculations. Inorganic carbon drawdown owing to organic matter production was calculated from measured changes in DIC and alkalinity according to: $\Delta\text{DIC}_{\text{org}} = |\Delta\text{DIC}| - 0.5|\Delta\text{TA}|$, where TA is total alkalinity. ΔDIC was corrected for CO₂ air-sea gas exchange following ref. 34 with chemical enhancement factors given in ref. 35. ΔTA was calculated from changes in DIC and pCO₂ using stoichiometric dissociation constants given in ref. 36. Calcium carbonate precipitation was estimated from alkalinity drawdown as $\Delta\text{DIC}_{\text{calc}} = 0.5(\Delta\text{TA} + \Delta\text{nitrate})$. Owing to strong wind and wave action in the fjord on day 12, some water in the mesocosms from below the halocline was mixed into the surface layer. Because surface water was lower in salinity, pCO₂, DIC and total alkalinity owing to the initial freshwater addition, injection of deep water led to a slight increase in pCO₂ (Fig. 1a), DIC and total alkalinity on this day. This also affected the calculations of $\Delta\text{DIC}_{\text{org}}$, $\Delta\text{C}_{\text{loss}}$ (Fig. 3a, b) and $\Delta\text{DIC}_{\text{calc}}$ (Supplementary Fig. 3).

Biogenic calcification. Inorganic carbon drawdown owing to biogenic calcification ($\Delta\text{DIC}_{\text{calc}}$) calculated from changes in surface layer alkalinity showed no distinct CO₂ treatment difference during bloom development (Supplementary Fig. 3). Although calcification continued for some days after the peak of the

bloom, this was not depicted in the alkalinity measurements owing to mixing in of higher alkalinity deep water on day 12. Because mixing across the halocline was similar in all CO₂ treatments, the divergence of estimated $\Delta\text{DIC}_{\text{calc}}$ however, indicates a CO₂ effect on calcification after the peak of the bloom. This phase of an *E. huxleyi* bloom, in which nutrient limitation impedes further cell division, is often characterized by excess calcification, leading to shedding of calcite platelets (coccoliths) and their accumulation in the water column. Overall, *E. huxleyi* cell numbers remained much below those typically observed in blooms of this species, which explains the comparatively low amount of calcium carbonate precipitation.

Excess carbon sequestration. Provided that the mechanisms underlying the observed CO₂ sensitivity of carbon consumption and carbon-to-nutrient stoichiometry can be generalized to other diatom- and coccolithophore-dominated new production systems, the excess CO₂ sequestration potential by the ocean's biological carbon pump was calculated for the periods from 1750 to present, and from 1750 to 2100 assuming: business-as-usual CO₂ emissions (IS92a¹⁰) until the end of this century; present-day oceanic carbon export of 12 Pg C yr⁻¹ (current estimates range between 8 Pg C yr⁻¹ and 16 Pg C yr⁻¹)³⁷; and an e-folding time of 100 yr for CO₂ sequestered by biological carbon export to get back into contact with the atmosphere³⁸.

Supplementary Fig. 4a depicts $\Delta\text{DIC}_{\text{org}}$ as a function of atmospheric pCO₂, with the present day value ($\Delta\text{DIC}_{\text{org}}$ at 380 μatm) set to 1. Extrapolating the observed trend to pre-industrial CO₂ levels (pCO₂ = 280 μatm) yields a value of ~0.95; that is, for a given amount of inorganic nutrients, biological carbon consumption under pre-industrial conditions was about 95% of today's level. On the basis of this relationship, an increase in atmospheric CO₂ from 280 μatm to 380 μatm (present day) corresponds to an excess carbon sequestration of 22 Pg (range 14–29 Pg) for the past 150 yr (Supplementary Fig. 4b). Without this negative feedback mechanism, atmospheric CO₂ would be approximately 11 μatm higher than its present value. By the end of this century, this process would sequester an additional 94 Pg C to the deep ocean, bringing total excess carbon sequestration to 116 Pg C (range 76–154 Pg C). This reduces the increase in atmospheric CO₂ by a total of 58 μatm at 2100.

26. Wanninkhof, R. & Thoning, K. Measurement of fugacity of CO₂ in surface water using continuous and discrete sampling methods. *Mar. Chem.* **44**, 189–205 (1993).
27. Gran, G. Determination of the equivalence point in potentiometric titrations of seawater with hydrochloric acid. *Oceanol. Acta* **5**, 209–218 (1952).
28. Johnson, K. M., Williams, P. J., Brandstrom, L. & Sieburth, J. McN. Colometric total carbon analysis for marine studies: automation and calibration. *Mar. Chem.* **21**, 117–133 (1987).
29. Barlow, R. G., Cummings, D. G. & Gibb, S. W. Improved resolution of mono- and divinyl chlorophylls *a* and *b* and zeaxanthin and lutein in phytoplankton extracts using reverse phase C-8 HPLC. *Mar. Ecol. Prog. Ser.* **161**, 303–307 (1997).
30. Mackey, M. D., Mackey, D. J., Higgins, H. W. & Wright, S. W. CHEMTAX — a program for estimating class abundances from chemical markers: application to HPLC measurements of phytoplankton. *Mar. Ecol. Prog. Ser.* **144**, 265–283 (1996).
31. Hansen, H. P. & Koroleff, F. in *Methods of seawater analysis* 3rd edn (eds Grasshoff, K., Kremling, K. & Ehrhardt, M.) 159–228 (Wiley VCH, Weinheim, 1999).
32. Holmes, R. M., Aminot, A., Kérouel, R., Hooker, B. A. & Peterson, B. J. A simple and precise method for measuring ammonium in marine and freshwater ecosystems. *Can. J. Fish. Aquat. Sci.* **56**, 1801–1808 (1999).
33. Qian, J. & Mopper, K. Automated high-performance, high-temperature combustion total organic carbon analyser. *Anal. Chem.* **68**, 3090–3097 (1996).
34. Delille, B. et al. Response of primary production and calcification to changes of pCO₂ during experimental blooms of the coccolithophorid *Emiliania huxleyi*. *Glob. Biogeochem. Cycles* **19**, GB2023 (2005).
35. Kuss, J. & Schneider, B. Chemical enhancement of the CO₂ gas exchange at a smooth seawater surface. *Mar. Chem.* **91**, 165–174 (2004).
36. Zeebe, R. E. & Wolf-Gladrow, D. CO₂ in seawater: equilibrium, kinetics, isotopes. *Elsevier Oceanogr. Ser.*, **65**, (Elsevier, Amsterdam, 2001).
37. Oschlies, A. Model-derived estimates of new production: new results point towards lower values. *Deep-Sea Res.* **48**, 2173–2197 (2001).
38. Maier-Reimer, E., Mikolajewicz, V. & Winguth, A. Future ocean uptake of CO₂: interaction between ocean circulation and biology. *Clim. Dynam.* **12**, 711–721 (1996).